Test Beam Measurements of an Irradiated Prototype Pixel Sensor Designed for the CEPC Vertex Detector

Y. Han[a,b,c], H. Zhu[a,c,*], X. Ai[a,c], M. Fu[f], R. Kiuchi[a,c], Y. Liu[d], Z. Liu[a,b,c], X. Lou[a,b,g], Y. Lu[a,c], Q. Ouyang[a,b,c], X. Shi[a,c], J. Tao[a,b,c], K. Wang[a,c], N. Wang[a,c], C. Yang[c,e], T. Yang[a,b,c], Y. Zhang[a,c], Y. Zhou[a,c]

[a] *Institute of High Energy Physics, Chinese Academy of Sciences, 19B Yuquan Road, Shijingshan District, Beijing, China*
[b] *University of Chinese Academy of Sciences, No.19(A) Yuquan Road, Shijingshan District, Beijing, China*
[c] *State Key Laboratory of Particle Detection and Electronics, 19B Yuquan Road, Shijingshan District, Beijing, China*
[d] *Deutsches Elektronen-Synchrotron (DESY), Notkestrasse 85 D-22607 Hamburg, Germany*
[e] *University of Science and Technology of China, No.96, JinZhai Road Baohe District, Hefei, Anhui, China*
[f] *Ocean University of China, No.238 Songling Road, Qingdao 266100, China*
[g] *Physics Department, University of Texas at Dallas, Richardson TX, USA*

Abstract

The Circular Electron Positron Collider (CEPC) has been proposed as a Higgs factory to measure the properties of the Higgs boson with unprecedented precision and to guide the search for new physics. To meet the stringent physics requirements, it is necessary to design and construct its vertex detector with the state-of-the-art silicon detector technologies. The first prototype CMOS pixel sensor, named JadePix-1, was developed for the CEPC vertex detector and its performance was first characterized with radioactive sources in laboratory. This prototype sensor was further characterized at the DESY test beam facility. Results are reported on the charge collection, cluster size, position resolution and detection efficiency before and after the sensor samples exposed to the neutron irradiation up to the fluence level of 10^{13} 1 MeV n_{eq}/cm^2.

Keywords: CEPC, JadePix-1, Test Beam, Neutron Irradiation

*Corresponding author
Email address: zhuhb@ihep.ac.cn (H. Zhu)

1. Introduction

The proposed Circular Electron Positron Collider (CEPC) [1, 2] will primarily operate at the center-of-mass energy of $\sqrt{s} = 240$ GeV as a Higgs factory. It will allow for precision measurement of the properties of the Higgs boson with high precision beyond the Large Hadron Collider (LHC) [3] and its successor, the High Luminosity LHC (HL-LHC) [4, 5]. The CEPC vertex detector will play a critical role in heavy flavor tagging and τ-lepton tagging that are vital for the precision physics program. It must be constructed with the state-of-the-art silicon detector technologies, and provide a high spatial resolution better than 3 μm, a low power consumption below 50 mW/cm^2 to allow forced air cooling, and a low material budget below 0.15% X/X_0 for each detector layer. This vertex detector must also survive a Total Ionizing Dose (TID) of 10 MRad and a Non-Ionizing Energy Loss (NIEL) of 2×10^{13} 1 MeV n_{eq}/cm^2 at its inner most layer over 10 years of operation. The first prototype pixel sensor for the CEPC vertex detector, named JadePix-1, was developed with a 0.18 μm CMOS imaging sensor process [6]. The prototype sensor was 7.8×3.8 mm^2 in size and contained pixel arrays of different pixel designs. It was aimed to optimize sensor diode geometries to achieve high charge-over-capacitance ratio, hence to reduce its analogue power consumption [7]. Its charge collection performance was first characterized with radioactive sources of ^{55}Fe and ^{90}Sr in laboratory [8]. In this paper, test beam results on charge collection, cluster size, position resolution and detection efficiency are reported for the JadePix-1 sensors before and after exposed to the neutron irradiation up to the fluence level of 10^{13} 1 MeV n_{eq}/cm^2. This paper is organized as follows: the neutron irradiation of the sensor samples is described in Sec. 2, then the experimental setup for the electron beam test is explained in Sec. 3, followed by the offline event reconstruction in Sec. 4. Measurement results are discussed in detail in Sec. 5. It is concluded with a summary and outlook in Sec. 6.

2. Neutron Irradiation

The neutron irradiation was performed at the Xi'an pulse reactor (XAPR) facility located at the Northwest Institute of Nuclear Technology (Xi'an, China). Bare JadePix-1 sensor samples were left unpowered and irradiated at room temperature. Three batches of samples were exposed to the fluence levels of 10^{12}, 5×10^{12} and 10^{13} 1 MeV n_{eq}/cm^2, respectively, and with an average fluence uncertainty of $\pm5\%$ and a neutron beam homogeneity of $\pm10\%$ as measured at the radiation facility. At each neutron fluence level, three JadePix-1 sensors were irradiated at the same time. The neutron flux was about 1.33×10^8 n/cm^2 per second and the neutron-to-γ ratio was controlled to be high enough so that the total ionization dose was not significant even after reaching the highest neutron fluence level. These irradiated samples were kept in quarantine to allow the neutron activation effects to die down. In-pixel circuit gain for each irradiated sensor was calibrated with a radioactive source of ^{55}Fe in laboratory before brought to the electron test beam facility.

3. Experimental Setup

JadePix-1 prototype pixel sensors were characterized with a EUDET-type beam telescope [9] operated at the DESY-II test beam facility [10], and data were taken at the electron beam energy of 4.4 GeV with an expected particle rate of about 3 kHz. The EUDET-type beam telescopes are tabletop tracking detectors with six high-precision MIMOSA26 pixel sensors, four scintillators with photo multiplier tubes (PMTs) for trigger purposes, a Trigger Logic Unit (TLU) [11] providing trigger logic and time stamp information on particle passage, and a data acquisition system for the readout. JadePix-1 prototype sensors were inserted as the Device Under Test (DUT) between the two arms of the beam telescope. During operation, one JadePix-1 sensor was mounted in an aluminum shielding box, which featured a beam window around the position of the sensor location to minimize the material budget and and the shielding box itself was mounted on a PI XY motorized stage. Lightproof Kapton foils of 50

μm thickness were used to protect the sensor on each side of the shielding box. The total DUT material budget, including the 250 μm thick DUT sensor, was estimated to be below 0.3% X/X_0.

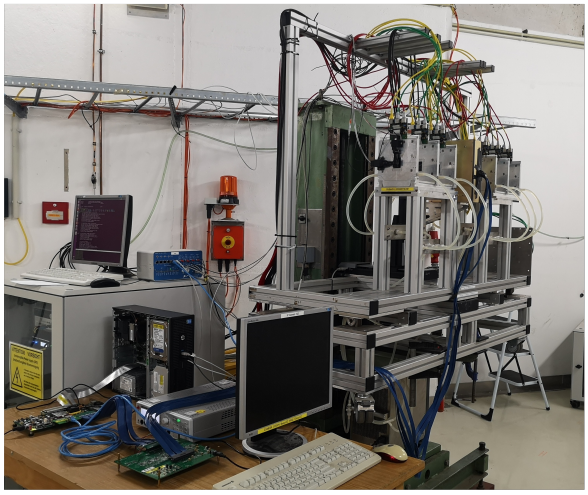

Figure 1: Beam telescope setup with a JadePix-1 sensor placed in an aluminum shielding box, which was mounted on an XY stage between the two arms of pixel reference planes.

Pixel sectors on the JadePix-1 prototype sensor, with 33×33 μm^2 pixels arranged in 48 columns and 16 rows, were enabled one at a time and read out in the rolling shutter mode at a clock frequency of 2 MHz. The readout electronics consisted of a daughterboard and a motherboard. The daughterboard was to amplify the single-ended analogue signal from the DUT sensor and converted it to a differential signal. The motherboard then digitized the signal from the daughterboard using multiple high-precision 16-bit analog-to-digital converters (ADCs). It also provided powering for the daughterboard and the DUT sensor. As a part of the data acquisition (DAQ) system, a commercial FPGA board (KC705) was deployed to read in the digitized signals from the motherboard, assembled data into event frames and stored them in buffer. After receiving the trigger signal from the TLU, the current frame together with one frame before and one after, were attached with the Trigger ID and written

out to the controller PC. The DUT data and data from the reference planes were synchronized with the Trigger ID and integrated into events within the EUDAQ [12], which was designed as a modular cross-platform data acquisition framework and widely used for beam tests.

4. Offline Track Reconstruction

Offline reconstruction and analysis of the test beam data were performed with the EUTelescope software package [9], consisting of the steps of raw data conversion, clustering, hit making, alignment and track fitting. After the raw data conversion, the clustering was performed by grouping pixels with charge above certain thresholds. Based on the clustered pixels, the hit position was determined using the Center of Gravity (CoG) method with the η-correction applied. Tracks were then reconstructed with the General Broken Lines (GBL) algorithm [13, 14], with both the multiple scattering effect and the energy loss taken into account. Precise alignment of the telescope reference planes and the DUT sesnor was achieved by minimizing track residuals using the Millepede-II algorithm [15].

5. Results and Discussion

Using the experimental setup and offline reconstruction described above, JadePix-1 sensors before and after the neutron irradiation were tested for their charge collection, position resolution and detection efficiency.

5.1. Charge Collection

Beam particles impinging the DUT sensor would deposit energy and generate electron-hole pairs along their paths through the sensor active volume. Generated charge carriers would be then collected by the N-well electrode[1] primarily via diffusion with a typical collection time close to 100 ns. Figure 2a

[1] In the JadePix-1 design, the PN-junction was formed by the high-resistivity P-type epitaxial layer and the N-well implant, and the latter served as the collection electrode.

shows an example distribution of the amount of charge collected in a seed pixel. Here a seed pixel was simply defined as the pixel collecting the highest amount of charge within a 5×5 pixel array and above the seed threshold of 100 e^-. The collected charge followed roughly the Landau distribution, and the most probable value (MPV) extracted from the Landau fit was taken as the representative collected charge. Measurements were performed for the DUT sensors with a pixel size of 33×33 μm^2 but different electrode sizes, in particular A1 with an electrode of 4 μm^2 and A3 with 15 μm^2, respectively. Measurements were repeated for the DUT sensors after the neutron irradiation.

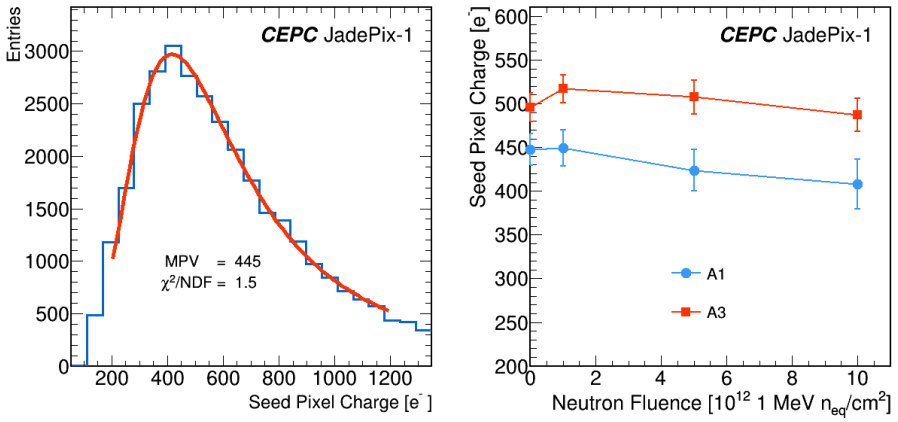

(a) (b)

Figure 2: (a) Distribution of charge collected in the seed pixels and fitted with a Landau function; (b) Seed pixel charge for pixels with a small electrode (A1 in blue bullet) and a large electrode (A3 in orange square) before and after neutron irradiation.

Figure 2b shows the decreased amount of charge collected by the seed pixels as the fluence increases. It shows that the DUT sensor with a larger electrode, *i.e.* A3, yielded higher radiation tolerance than A1, which could be explained by the lower trapping probability due to the shorter collection distance. In addition, noise level was measured for each DUT sensor in the absence of any external signal. After the neutron irradiation up to 10^{13} 1 MeV n_{eq}/cm^2, the Equivalent Noise Charge (ENC) value increased from 7.0 e^- to 8.3 e^- for A1,

and 9.5 e^- to 10.7 e^- for A3, respectively. After the neutron irradiation, sensors with a small electrode yielded a higher S/N ratio and hence a larger Q/C. This could lead to a lower analogue power consumption, which would be preferred for the sensor design.

5.2. Cluster Size

Clusters were constructed by searching for pixels around the seed pixel and with the collected charge above the neighbor threshold of $3\sigma_{\text{noise}}$. Due to the existence of diffusion, some of the charge carriers could end up in the neighboring pixels. Such charge sharing could be affected by the hit position and incident angle of the track with respect to the DUT sensor surface. During the test beam operation, DUT sensors were placed nearly perpendicularly to the beam and illuminated almost uniformly with electrons. Therefore these two effects were minimized and not analyzed specifically. Figure 3a shows the cluster size distributions of an example DUT sensor, peaking at three pixels in both x and y directions. And Figure 3b shows that the average cluster sizes are smaller for pixel sensors with a larger electrode. This can be explained that with a larger electrode, charge carriers would be more likely to be collected in the incident pixel and fewer of them would spread into the neighboring pixels. It also shows that due to the increased trapping probability after the neutron irradiation, the average cluster size decreased at a higher fluence level.

5.3. Position Resolution

With the test beam data, the position resolution of a DUT JadePix-1 sensor can be evaluated with the following formula:

$$\sigma_{\text{pix}} = \sqrt{\sigma_{\text{res}}^2 - \sigma_{\text{tel}}^2} \tag{1}$$

where σ_{res} is the standard deviation of the residual distribution and σ_{tel} the beam telescope resolution at the DUT sensor surface. The residual is defined as the difference between the measured DUT hit position and the unbiased track fit using the measured hits from the reference planes only and extrapolated

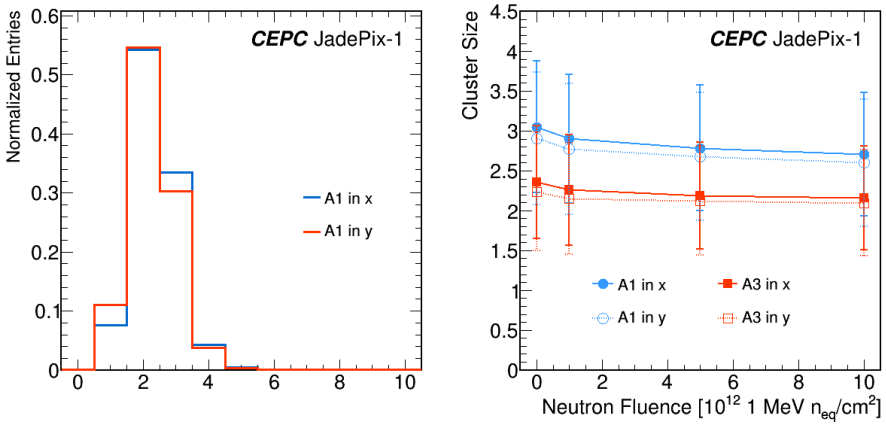

(a) (b)

Figure 3: (a) Cluster size distributions for an example DUT sensor in the x and y directions; (b) average cluster sizes for sensors with a small electrode (A1 in x and y with blue open and closed bullets) and a large electrode (A3 in x and y with orange open and closed squares) before and after the neutron irradiation.

to the DUT sensor surface. Figure 4a shows the residual distribution of an example DUT sensor in the x direction and fitted with a Gaussian function. For a given beam telescope setup for JadePix-1, including the DUT position and its material budget, σ_{tel} was evaluated to be around 4.5 μm using the GBL Track Resolution Calculator [16]. Beam energy and position resolution for the reference planes were varied within their uncertainties to assess their impacts and propagated to the determined position resolutions. Figure 4b shows that the position resolutions of the DUT sensors with a small electrode (A1) degraded from around 3.5 μm to 5 μm due to reduced charge sharing after neutron irradiation, but remained nearly unchanged at around 3 μm for the DUT sensor with a large electrode (A3).

5.4. Detection Efficiency

The overall detection efficiency was calculated using the tracks passing through the DUT sensor, but with the area near the pixel array edge excluded. A matched track was indentified if there was a hit within the distance of $|x, y_{\text{hit}} -$

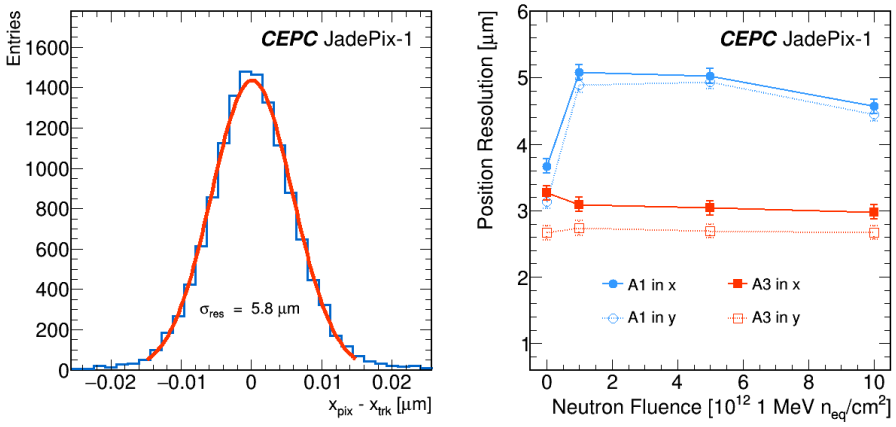

(a) (b)

Figure 4: (a) Residual ($x_{\rm pix} - x_{\rm trk}$) distribution of an example DUT sensor in the x direction; (b) position resolution for sensors with a small electrode (A1 in x and y with blue open and closed bullets) and a large electrode (A3 in x and y with orange open and closed squares) before and after the neutron irradiation.

$x, y_{\rm trk}| < 33$ μm (corresponding to the pixel pitch), with respect to the extrapolated position from the telescope track to the DUT sensor surface. The detection efficiency can be simply define as follows:

$$\epsilon = \frac{N_{\rm matched}}{N_{\rm tracks}} \tag{2}$$

It should be stressed that the overall efficiency represented the combined efficiencies of the DUT sensor and the DAQ system. Unfortunately, there was an issue observed with the DAQ system. During the data-taking, the DUT data were stored temporarily in the memory on the FPGA board. Upon receiving the trigger signal from the TLU, three consecutive data frames with the triggered frame in the middle, would be recorded on the hard disk. The long integration time of the reference planes (around 230 μs for two consecutive frames) could cause problems for the data-taking. When the first track hit the scintillators and triggered the data recording, a second track might hit the DUT sensor. If the second track arrived out of the DUT recording time window (around 50 μs)

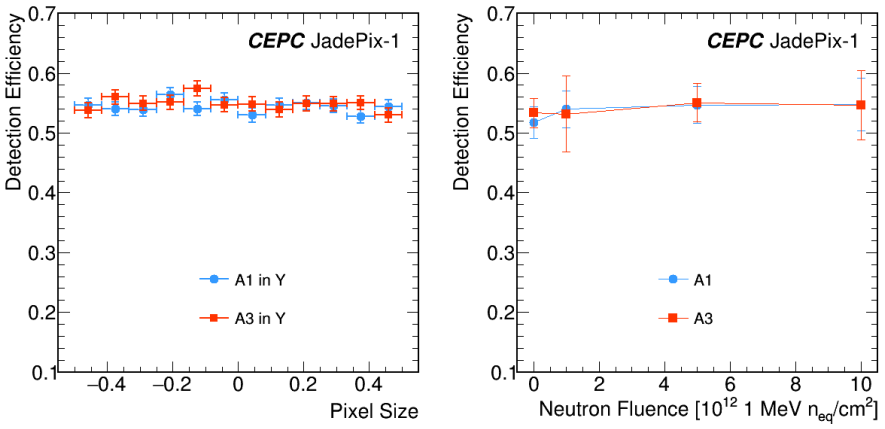

(a) (b)

Figure 5: (a) Detection efficiencies for two example DUT sensors projected into a pixel; (b) detection efficiencies for the DUT sensors with a small electrode (A1 in blue bullets) and a large electrode (A3 in red squares) before and after the neutron irradiation.

but still within the long integration time of the reference planes, the track on the DUT sensor could not be recorded and this would result in artificial detection inefficiency. Figure 5a shows the rather low but nearly flat detection efficiencies projected into one pixel for example DUT sensors. Figure 5b shows the detection efficiencies for the DUT sensors before and after the neutron irradiation. Large systematic uncertainties were assigned to cover the run-to-run efficiency dispersion caused by the DAQ inefficiency that was understood to be also particle-rate dependent. No detection efficiency drop was observed even after the neutron irradiation up to the fluence level of 10^{13} 1 MeV n_{eq}/cm^2. This might be explained by the low seed pixel charge threshold of 140 e^- that was required to register a hit. However, this shall change for sensors to be developed with complex in-pixel electronics, for which a higher threshold must be deployed to suppress the increased electronics noise and this would cause detection efficiency loss after irradiation.

6. Summary and Outlook

The first prototype CMOS pixel sensor, named JadePix-1, was developed for the CEPC vertex detector. Its performance before and after the neutron irradiation up to the fluence level of 10^{13} 1 MeV n_{eq}/cm^2 was characterized at the DESY test beam facility. Degraded performance on charge collection, cluster size and position resolution were observed after the neutron irradiation. Sensors with a large electrode were more radiation tolerant, but sensors with a small electrode could yield a higher Q/C and thus lower analogue power consumption. Due to the DAQ system imperfection, the obtained efficiencies could not fully represent the detection efficiencies of the DUT sensors. No detection efficiency drop was observed even up to the highest fluence level, which might be explained by the rather low seed pixel charge threshold. In the meantime, several prototype CMOS pixel sensors [17] with complex in-pixel electronics and novel readout architectures are being developed. It is foreseen to deliver a full-size pixel sensor that can fulfill all the stringent requirements of the CEPC vertex detector in the years to come.

7. Acknowledgement

This project is jointly supported by the National Natural Science Foundation of China (No.11505207, No.11573028), the State Key Laboratory of Particle Detection and Electronics, the CAS Center for Excellence in Particle Physics (CCEPP), the IHEP Innovation Grant (Y4545170Y2), the CAS International Partnership Program and the CAS Special Grant for Large Scientific Projects (113111KYSB20170005). The measurements leading to these results have been performed at the Test Beam Facility at DESY Hamburg (Germany), a member of the Helmholtz Association (HGF).

References

[1] The CEPC Study Group, CEPC Conceptual Design Report: Volume 1 - Accelerator (IHEP-CEPC-DR-2018-01, IHEP-AC-2018-01). arXiv:1809.00285.

[2] The CEPC Study Group, CEPC Conceptual Design Report: Volume 2 - Physics & Detector (IHEP-CEPC-DR-2018-02, IHEP-EP-2018-01, IHEP-TH-2018-01). arXiv:1811.10545.

[3] L. Evans and P. Bryant, LHC Machine, JINST 3 (2008) S08001. doi:10.1088/1748-0221/3/08/S08001.

[4] G. Apollinari, et al., High Luminosity Large Hadron Collider HL-LHC, CERN Yellow Rep. (5) (2015) 1–19. arXiv:1705.08830.

[5] ATLAS and CMS Collaborations, Report on the Physics at the HL-LHC and Perspectives for the HE-LHC, CERN Yellow Rep. Monogr. 7. arXiv:1902.10229.

[6] Y. Zhang, et al., Charge collection and non-ionizing radiation tolerance of CMOS pixel sensors using a 0.18 μm CMOS process, Nucl. Instrum. Meth. A831 (2016) 99–104. doi:10.1016/j.nima.2016.03.031.

[7] W. Snoeys, Monolithic pixel detectors for high energy physics, Nucl. Instrum. Meth. A731 (2013) 125–130. doi:10.1016/j.nima.2013.05.073.

[8] L. Chen, et al., Characterization of the first prototype CMOS pixel sensor developed for the CEPC vertex detector, Radiat. Detect. Technol. Methods 3 (2019) 45. doi:https://doi.org/10.1007/s41605-019-0124-0.

[9] H. Jansen, et al., Performance of the EUDET-type beam telescopes, EPJ Tech. Instrum. 3 (1) (2016) 7. arXiv:1603.09669, doi:10.1140/epjti/s40485-016-0033-2.

[10] R. Diener, et al., The DESY II Test Beam Facility, Nucl. Instrum. Meth. A922 (2019) 265–286. arXiv:1807.09328, doi:10.1016/j.nima.2018.11.133.

[11] D. Cussans, A Trigger/Timing Logic Unit for ILC Test-beamsdoi:10.5170/CERN-2007-007.420.
URL http://cds.cern.ch/record/1091502

[12] P. Ahlburg, et al., EUDAQ - A Data Acquisition Software Framework for Common Beam Telescopes, arXiv:1909.13725.

[13] C. Kleinwort, General Broken Lines as advanced track fitting method, Nucl. Instrum. Meth. A673 (2012) 107–110. arXiv:1201.4320, doi:10.1016/j.nima.2012.01.024.

[14] V. Blobel, C. Kleinwort, F. Meier, Fast alignment of a complex tracking detector using advanced track models, Comput. Phys. Commun. 182 (2011) 1760–1763. arXiv:1103.3909, doi:10.1016/j.cpc.2011.03.017.

[15] V. Blobel, Software alignment for tracking detectors, Nucl. Instrum. Meth. A566 (2006) 5–13. doi:10.1016/j.nima.2006.05.157.

[16] S. Spannagel and H. Jansen, GBL Track Resolution Calculator v2.0, doi:10.5281/zenodo.48795.

[17] H. Zhu, Vertex and Tracking Detectors for the Circular Electron Positron Collider (CEPC), JINST 373 (2020) PoS(Vertex2019)046.